Published in final edited form as:
Nat Chem Biol. 2015 December ; 11(12): 973–980. doi:10.1038/nchembio.1952.

A selective chemical probe for exploring the role of CDK8 and CDK19 in human disease

Trevor Dale[#2,*], **Paul A. Clarke**[#1,*], **Christina Esdar**[3], **Dennis Waalboer**[1], **Olajumoke Adeniji-Popoola**[1], **Maria-Jesus Ortiz-Ruiz**[1], **Aurélie Mallinger**[1], **Rahul S. Samant**[1], **Paul Czodrowski**[3], **Djordje Musil**[3], **Daniel Schwarz**[3], **Klaus Schneider**[3], **Mark Stubbs**[1], **Ken Ewan**[2], **Elizabeth Fraser**[2], **Robert TePoele**[1], **Will Court**[1], **Gary Box**[1], **Melanie Valenti**[1], **Alexis de Haven Brandon**[1], **Sharon Gowan**[1], **Felix Rohdich**[3], **Florence Raynaud**[1], **Richard Schneider**[3], **Oliver Poeschke**[3], **Andree Blaukat**[3], **Paul Workman**[1], **Kai Schiemann**[3], **Suzanne A. Eccles**[1], **Dirk Wienke**[3,*], and **Julian Blagg**[1,*]

[1]Cancer Research UK Cancer Therapeutics Unit, The Institute of Cancer Research, London, SW7 3RP

[2]School of Bioscience, Cardiff University, Cardiff, UK

[3]Merck KGaA, Merck Serono, Darmstadt, Germany

[#] These authors contributed equally to this work.

Abstract

There is unmet need for chemical tools to explore the role of the Mediator complex in human pathologies ranging from cancer to cardiovascular disease. Here we determine that CCT251545, a small molecule WNT-pathway inhibitor discovered through cell-based screening, is a potent and selective chemical probe for the human Mediator complex-associated protein kinases CDK8 and CDK19 with >100-fold selectivity over 291 other kinases. X-ray crystallography demonstrates a Type 1 binding mode involving insertion of the CDK8 C-terminus into the ligand binding site. In

[*]Corresponding authors julian.blagg@icr.ac.uk; paul.clarke@icr.ac.uk; daletc@cardiff.ac.uk and dirk.wienke@merckgroup.com.

Author contributions

J.B., A.M., Ka.S. and D.Wa. designed and synthesised all new compounds; P.C. and D.M. analysed crystallographic data; D. S. performed SPR experiments; G.B., W.C., K.E., E.F., S.G., O.A.P., RteP., M.O.R., M.S. and R.S.S. developed and performed cell-based assays; K.E., A.H.B. and M.V. performed *in vivo* studies. A.B., P.A.C., T.D., C.E., S.A.E., A.M., F.Ro., F.Ra., Ka.S, Kl.S., R.S., P.W., D.W. and J.B designed studies and analysed results. J.B., P.A.C., T.D. and D.W. wrote the paper.

Accession codes

Protein Data Bank (PDB): coordinates and structure factors for the co-crystal structure CDK8/Cyclin C: CCT251545 have been deposited with accession code 5BNJ; Microarray data are available on the NCBI Gene Expression Omnibus (GEO) website under accession number GEO GSE67849.

Competing Financial Interests.

T.D., P.A.C., W.C., D.W., O.A.P., M.O.R., A.M., R.S.S., M.S., E.F., RteP., A.H.B., M.V., G.B., S.G., F.Ra., P.W., S.A.E. and J.B. are current or former employees of The Institute of Cancer Research, which has a commercial interest in the development of WNT pathway inhibitors. C.E., P.C., F.Ro., D.M., Ka.S., Kl.S., R.S., O.P., A.B. and D.W. are current or former employees of Merck Serono, which has a commercial interest in the development of WNT pathway inhibitors.

Additional Information

Supplementary information, compound synthetic methods and chemical probe information is available in the online version of the paper.

Europe PMC Funders Author Manuscripts

contrast to Type II inhibitors of CDK8/19, CCT251545 displays potent cell-based activity. We show that CCT251545 and close analogues alter WNT-pathway regulated gene expression and other on-target effects of modulating CDK8/19 including genes regulated by STAT1. Consistent with this we find that phosphorylation of STAT1^{SER727} is a biomarker of CDK8 kinase activity *in vitro* and *in vivo*. Finally, we demonstrate *in vivo* activity of CCT251545 in WNT-dependent tumors.

INTRODUCTION

The discovery of chemical probes based on testing libraries of small molecules against cellular pathway screens has re-emerged as a credible hit discovery strategy, particularly for signalling networks lacking well-validated druggable targets. The success of these approaches is highly dependent upon the quality of the cell-based assay cascade and the chemical library in order to minimise false-positive responses[1,2]. Subsequent hit series optimisation and proximal biomarker discovery are greatly facilitated by identification of the molecular targets and this, in turn, requires design and synthesis of appropriate chemical tools for target pull-down and cellular proteomics[3-5]. Cell-based screening approaches have the potential for discovery of cell-penetrant chemical matter that elicits a desired cellular response and have been instrumental to hit discovery for 37% of FDA-approved first-in-class drugs between 1999-2008[6]. Recent notable successes include the tankyrase inhibitor XAV939[7] and porcupine inhibitor LGK974[8] that have rekindled cell biology and drug discovery interest in WNT signalling[9].

We previously reported a series of 3,4,5-trisubstituted pyridines identified from a high-throughput cell-based reporter assay of WNT signalling; optimisation to CCT251545 (**1**) (Fig. 1a) provided preliminary evidence for *in vivo* activity[10]. However, we recognised that identification of the molecular target(s) would accelerate further progress; for example, by enabling the discovery of proximal pharmacodynamic biomarkers with which to establish direct target engagement *in vivo*. Using a cell-based assay cascade in which WNT signalling is activated at distinct loci, we had previously established that **1** acts at or below T-cell factor (TCF)[10]. Regulation of β-catenin/TCF transcription involves recruitment or loss of DNA binding proteins, histone modification and interaction with additional protein networks such as the Mediator complex that provide the link between gene-specific regulators and basal transcriptional machinery[11-14]. Given the complexity of these multiple networked interactions in the β-catenin/TCF locale, a candidate-based investigation to identify the molecular targets of **1** was impractical and we therefore adopted an unbiased chemical proteomics approach.

Herein we report the molecular targets of the 3,4,5-trisubstituted pyridine series – namely the Mediator complex-associated, cyclin-dependent kinases CDK8 and CDK19 – and the characterisation of CCT251545 as a potent and selective chemical probe suitable for cell-based and *in vivo* exploration of the reported context-dependent roles of CDK8/19 and associated kinase module subunits in human disease and other biological settings[15-17].

Europe PMC Funders Author Manuscripts

RESULTS

Target Identification

To identify the molecular target(s) of the 3,4,5-trisubstituted pyridine series, we prepared a set of derivatives to enable Cellular Target Profiling® from cell lysates of LS174T human colon carcinoma cells that harbor an activating β-catenin mutation (http://www.kinaxo.de/). Cognisant of the potency and structure-activity-relationships of **1**, morpholine analogue **2** and *N*-methyl piperazine **3** in a cell-based reporter assay of WNT signalling[10], we hypothesised that substitution from the terminal piperazine nitrogen of **3** would maintain activity. *N*-Propyl piperazine **4** demonstrated toleration of a linker along this vector and the extended derivative **5** retained cellular potency and enabled coupling to sepharose beads generating an affinity matrix. LS174T cells were grown in media with different isotopically-labelled amino acids; target proteins were then captured from lysates by the compound **5** affinity matrix before displacement by unconjugated **4**, active non-basic indazole **6** or, as a non-displacing control, inactive *N*-propyl piperazine **7** that has a similar chemical structure and physicochemical properties to **4** (Supplementary Results, Supplementary Table 1). SILAC-based quantitative mass spectrometry facilitated identification of proteins that specifically interact with immobilised compound **5**, and determination of their affinities as previously described (Fig. 1b)[18]. In competition experiments, unconjugated analogues **4** and **6** were used at a range of concentrations (3 nM to 30 μM). Target profiling in competition with **4** revealed 53 potential target proteins, all of which showed concentration-dependent binding to the affinity matrix as well as concentration-dependent displacement by **4** with apparent K_d values between 3 nM and 23.9 μM (Fig. 1c and Supplementary Table 2). Of these, 18 were protein kinases, suggesting a binding preference for this protein family. We also identified proteins that have been strongly linked to WNT signalling, including AXIN2 and GSK3β; however, their affinities (K_d ~1 μM, Supplementary Table 2) were 2 orders of magnitude weaker than cell-based reporter activities in both 7dF3 and LS174T cells (Supplementary Table 1), suggesting that they are unlikely to mediate the observed cell-based activities. By contrast, CDK8 and CDK19 exhibited the highest affinities for compound **4** of the kinases identified in the displacement assay (K_d = 36 and 102 nM respectively).

CDK8, and its paralog CDK19, are transcription-regulating cyclin C-dependent kinases. CDK8 and CDK19 are components of the Mediator complex that provides a link between transcriptional regulators, the RNA polymerase II transcription machinery and gene-specific transcription; CDK8 or CDK19 form a 4-subunit subcomplex with cyclin C, MED12 and MED13 (commonly referred to as the kinase-module) that associates in a dynamic fashion with the rest of Mediator complex[13,19,20]. Consistent with these observations, we identified 20 additional Mediator complex components as proteins specifically isolated with immobilised compound **5** that were competed off by compound **4** with apparent K_d values < 100 nM (Fig. 1c and Supplementary Table 2). Competition with **6** also identified CDK8 and 19 as high-affinity specific binding proteins in the displacement assay (K_d = 49 and 14 nM respectively), together with 8 additional Mediator complex components (Supplementary Fig. 1 and Supplementary Table 3). By contrast, the structurally similar but inactive analog **7**

failed to compete with any components of Mediator complex including CDK8/19 (Supplementary Table 4).

Interestingly, both **4** and **6** interacted weakly (K_d = 0.407 – 0.578 μM) with three components of the PI(3,5)P_2, regulatory complex; 1-phosphatidylinositol-3-phosphate 5-kinase (PIKFYVE), phosphatidylinositol 3,5-bisphosphate 5-phosphatase (FIG4), and tax1-binding protein 2 (TAX1BP2). However, as inactive analog **7** also interacted with the same 3 components (K_d = 0.012 – 0.018 μM), we deduced that binding to these proteins is unlikely to contribute to cellular activity (Fig. 1c**,** Supplementary Fig. 1 and Supplementary Tables 2-4).

We concluded from these results that an affinity matrix comprising immobilised compound **5** selectively binds kinases CDK8/19. Interestingly, many components of the Mediator complex remain intact during the capture protocol, although we did not observe co-purification of any transcription factors such as β-catenin/TCF or components of the core RNA-Pol II machinery that have been shown to interact with the Mediator subunits[13]. Consistent with these observations, competitor compounds **4** and **6,** but not inactive control **7**, competitively displaced CDK8/19, other kinase module components, and additional Mediator complex partners from the affinity matrix. (Fig. 1c, Supplementary Fig. 1 and Supplementary Tables 2-4).

To examine the extent to which CDK8/19 binding explained the cell-based activity of the 3,4,5-trisubstituted pyridine series, we compared CDK8 kinase binding affinity with our previously reported 7dF3 and LS174T cell-based TCF/LEF WNT-reporter potencies for a series compounds of varying activity (Fig. 2a and Supplementary Fig. 2)[10]. The observed correlations (R^2 = 0.83 and 0.85 respectively), coupled with a strong correlation between CDK8 and CDK19 binding affinity across 3,4,5-trisubstituted pyridines (R^2 = 0.95, Fig. 2b), indicated that CDK8 and/or CDK19 are major contributors to the cell-based activity in both LS174T and 7dF3 cells. Similar binding affinity for both kinases is consistent with high sequence similarity between the CDK8/19 kinase domains; the closest non-conserved amino acid residues to the ATP binding site (Asp48, Ser80, Thr360 in CDK8; Glu, Ala and Asn respectively in CDK19) are remote (8 - 13 Å) and unlikely to directly influence ligand binding.

Confirmation of binding to CDK8 and CDK19

We used surface plasmon resonance (SPR) studies with full-length CDK8/cyclin C complex to confirm direct target binding for **1** (Fig. 2c). Reporter displacement assays against full-length CDK8/cyclin C and CDK19/cyclin C complexes were also used to determine compound K_d and binding kinetics (Supplementary Tables 5-6). Cellular thermal shift analysis (CETSA)[21] confirmed high affinity target engagement for **1** with both CDK8 and CDK19 in SW620 human colorectal cancer cells exhibiting constitutively active WNT signalling due to an inactivating *APC* mutation (Fig. 2d**,** Supplementary Fig. 3).

Selective pull-down of CDK8/19 from LS174T cell lysates by immobilised compound **5** is consistent with the selectivity profile of **1** when tested at 1 μM versus an additional panels of 291 kinases and 55 receptors, ion channels and enzymes[10]. GSK3α and β were the only hits

(IC_{50} = 0.462 and 0.690 μM respectively) consistent with the identification of GSK3α and β as weak interactors by SILAC (Kd = 1.75 and 1.59 μM respectively (Fig.1c and Supplementary Table 2). Importantly, there was no evidence for inhibition of CDKs 1-7 or 9 in the presence of their respective cyclin partners. Taken together, SILAC-mediated target identification, kinase selectivity data, biophysical methods (both *in vitro* and in cells) and the close correlation between kinase binding affinity and cellular activity suggest that CDK8/19, likely as part of a Mediator complex, are the molecular targets of the 3,4,5-trisubstituted pyridine series.

Type II inhibitors of CDK8/19

Interestingly, we observed that sorafenib – a reported inhibitor of CDK8/19 that confirmed in our hands (IC_{50} = 0.199±0.0205 and 0.206±0.0114 μM respectively) and for which X-ray crystallographic studies reveal a Type II binding mode (PDB code: 3rgf)[22] – did not exhibit potent cell-based activity in 7dF3 or LS174T reporter assays (Supplementary Table 7) and also did not demonstrate binding and stabilisation of CDK8 nor CDK19 in SW620 cells by CETSA analysis (Fig. 2d and Supplementary Fig. 3). We therefore investigated whether other Type II inhibitors of CDK8/19 lack translation to cell-based assays of WNT signalling. Biochemical screening of available clinical and preclinical kinase inhibitors with chemical structures consistent with a Type II binding mode revealed potent binding activity for ponatinib (Iclusig), a BCR-ABL inhibitor marketed for relevant leukaemias[23], and linifanib, a potent inhibitor of receptor tyrosine kinases in clinical studies[24]. Similar to sorafenib, we noted that *in vitro* potency of linifanib versus CDK8/cyclin C and CDK19/cyclin C (IC_{50} = 0.014±0.001 and 0.024±0.003 μM respectively) did not translate to potent inhibition of TCF reporter activity in 7dF3 or LS174T cells (IC_{50} = 1.29±0.489 and 5.170±0.887 μM respectively) nor to CDK8/19 binding in SW620 cells (CETSA), despite potent cell-based activity reported in the literature against other kinase targets[25,26]. For ponatinib, we observed improved translation to cell-based TCF reporter activity; however CETSA analysis in SW620 cells revealed minimal stabilisation of CDK8 or CDK19 at 0.30 μM – a 21-fold and 13-fold drop-off compared to *in vitro* potency – whereas compound **1** demonstrates > 50% stabilisation at 0.30 μM (Supplementary Table 7 and Supplementary Fig. 3**)**. Notably, linifanib and ponatinib exhibit longer residence times than sorafenib and **1** versus CDK8 (295, 512, 52 and 43 minutes respectively, Supplementary Table 5) and versus CDK19 (166, 413, 106 and 86 minutes respectively, Supplementary Table 6). Thus the better translation to cell-based potency observed for **1** cannot be attributed to longer target residence time. Cell-penetrant Type II kinase inhibitors do not compete with ATP[27] and are therefore less prone to reduced potency in cell-based assays; we were therefore interested to explore differences in CDK8-binding mode between **1** and sorafenib.

Structure of CDK8/cyclin C in complex with CCT251545

To investigate the mode of binding of 3,4,5-trisubstituted pyridines to CDK8, and potential differences from the reported sorafenib Type II binding mode, we obtained the crystal structure of **1** in complex with the kinase domain of CDK8 and cyclin C at 2.6 Å resolution (Pdb code: 5BNJ Fig. 3a and Supplementary Table 8). In this structure, CDK8 is observed in complex with cyclin C with the ligand occupying the ATP binding site. Binding of **1** to the kinase hinge region involves a hydrogen bond acceptor interaction of the pyridine nitrogen

Europe PMC Funders Author Manuscripts

with the NH of Ala100; the observed electron density also supports an interaction between C2-H of the pyridine ring and the carbonyl of Asp98. The 3-chloro substituent of the pyridine ring stacks against gatekeeper residue Phe97 and the amide of the spirolactam moiety bridges between the catalytic Lys52 and residue Asp173 of the DMG motif located at the N-terminus of the activation loop. Of particular note, we observe a torsion between the plane of the piperidine and pyridine rings consistent with our observation that such a conformation is important for activity of the 3,4,5-trisubstituted pyridine series in cell-based reporter assays[10]. The C5-phenylpyrazole substituent occupies the solvent channel, consistent with the maintained potency of **5** that bears an extended linker along this vector. Interestingly, the extended C-terminal chain of CDK8 is observed to reinsert adjacent to the hinge region in the presence of **1** with the guanidine side chain of Arg356 forming a cation-*pi* interaction with phenyl ring of the ligand (Fig. 3a, 3b). This interaction is consistent with previously reported SAR where strongly electron-withdrawing substituents on the phenyl ring abrogate activity[10]. We postulate that this unusual C-terminal Arg356 insertion into the hinge region may contribute to the exquisite kinase selectivity of **1**. Notably, the binding mode of **1** is significantly different from the published structure of sorafenib with CDK8 (pdb code 3rgf)[22] where a DMG-out orientation of the activation loop is observed, consistent with a type II binding mode and where the extended C-terminal tail including Arg356 is present in the crystallography construct but is not resolved (Fig. 3c). We hypothesise that the relatively poor translation into 7dF3 and LS174T cell-based reporter activity observed with sorafenib and other Type II CDK8 inhibitors may be a consequence of their Type II binding mode, suggesting that intracellular CDK8 is trapped in a tightly-bound active conformation either in a Mediator complex or a free 4-subunit kinase-module with slow equilibration to inactive kinase conformations. This notion is consistent with our observation that MED12, MED13 and an intact Mediator complex were captured by the affinity matrix containing compound **5**.

Compound-induced gene expression changes

We next explored how gene-expression changes induced by **1** correlated with those caused by silencing of CDK8 and/or CDK19. Colo205 human colorectal cancer cells harboring CDK8 amplification[28] were stably transduced with a doxycycline (dox)-inducible shRNA-expressing plasmid targeting CDK8 or a stable shRNA for CDK19. Following expression of the shRNAs, we observed a reduction in TCF-dependent reporter transcription, consistent with the observed effect of **1** on this cell line (Fig. 4a and Supplementary Fig. 4**)**. A similar reduction in TCF-dependent transcription was also observed in 7dF3 cells following treatment with enzymatically-synthesised siRNA (esiRNA) for CDK8 or CDK19 (Supplementary Fig. 5**)**. CDK8 protein was expressed from a dox-inducible promoter in a HEK293 cell line with low basal levels of TCF-dependent transcription. Wild-type, but not kinase-dead, CDK8 increased basal levels of TCF-reporter expression by 2-fold (Fig. 4b). Taken together, these data indicate that expression of an enzymatically active CDK8 is necessary and sufficient for activating a fraction of total β-catenin/TCF-dependent transcription.

We next examined a 3D culture model of murine intestinal-derived organoids expressing a transgenic dox-inducible mutant β-catenin[29]. In this model, loss of activated β-catenin

expression following removal of dox results in reduced WNT signalling with characteristic decreased expression of *Axin2*, *Ascl2*, *Myc* and *Tiam1* and increased expression of the enterocyte differentiation marker *Car4*, as determined by qRT-PCR (Fig. 5a). Treatment with **2**, a close analog of **1** with an equivalent pharmacological and kinase selectivity profile (Supplementary Tables 1, 9 and 10), gave a gene expression signature consistent with WNT signalling inhibition following loss of mutant β-catenin expression (Fig. 5a).

To identify broader patterns in transcriptional responses to our CDK8/19 inhibitors, gene expression microarray studies were performed using mRNA prepared from the same murine cell organoids expressing mutant β-catenin. The organoids were treated with **2**, analog **6 (**with an equivalent pharmacological and kinase selectivity profile to **2**, or inactive analog **8** (Supplementary Tables 9 and 11). Loss of activated β-catenin resulted in significantly ($p<0.001$) altered expression of 78 genes (Supplementary Figs. 6 – 8**)**. Consistent with inhibition of WNT signalling, 31 of the 78 genes, including *Axin2*, *Ascl2* and *Myc*, were known targets of WNT signalling. In agreement with the notion that our optimised 3,4,5-trisubstituted pyridines would not be general inhibitors of transcription, treatment with compound **2** or **6** resulted in significantly ($p<0.001$) altered expression of only 34 or 219 genes respectively (Supplementary Figs. 6 and 7). Importantly, inactive control **8** did not elicit any of the significant gene expression changes observed with **2** or **6**. Comparison with the expression profile resulting from loss of activated β-catenin confirmed that compounds **2** and **6** each inhibit WNT signalling (Fig. 5a**,** Supplementary Fig, 7a). Treatment with either active compound, but not inactive analogue **8**, also induced an additional set of transcriptional changes not shared by β-catenin removal. This included a ‘stress response’ gene expression signature that has been linked to NRF2 signalling and is consistent with literature reports that CDK8/19 may be involved in regulating stress response pathways (Supplementary Figs. 7 and 8)[30].

A further analysis of changes in mRNA abundance was also carried out in LS174T and COLO205 human colorectal cancer cells treated with **1** or **6** (Supplementary Fig. 9**)**. Comparing differentially expressed mRNAs following compound treatment to those modulated by overexpression of dominant negative TCF4 or following depletion of β-catenin by shRNA in LS174T cells[31] again identified a significant overlap with those transcripts altered in abundance by compound treatment (Fig. 5b). As in the organoids, not all of the changes in mRNA abundance resulting from compound treatment could be accounted for by modulation of WNT signalling. The overlap between the transcripts modulated in different cell lines and in response to our compounds was also incomplete which is unsurprising given the potentially pleiotropic effects of CDK8/19 modulation and the different genetic backgrounds of the cell lines selected for analysis. However, when we compared enrichment of transcription factor binding sites in genes encoding transcripts significantly altered in abundance, we found more similarity between the effects of compound treatment between LS174T and COLO205 cells (Fig. 5b and Supplementary data set 1). Of note, we identified enrichment of genes regulated by TCF4/LEF1 and additional transcription factors reliant on the Mediator complex and CDK8/19 (Supplementary data set 1). These included the STAT family of transcription factors[32], HIF1*a*[33], serum response factor (SRF) and SRF-dependent transcription factors like JUN[34] and also NRF2 that was detected in the organoid expression

profiling experiments (Supplementary Fig. 7 and 8). Pathway analysis (Supplementary data set 2) also indicated enrichment of transcripts from genes that encode proteins involved in pathways or processes regulated or influenced by CDK8/19 and the mediator complex – such as WNT, TGFβ, the inflammation and immune response, cell adhesion, the epithelial to mesenchymal transition and development – that are all regulated or influenced by CDK8/19 and the Mediator complex.

Overall, the gene expression changes we observed are consistent with our previous report identifying the 3,4,5-trisubstituted pyridine series as inhibitors of WNT signalling in the TCF locale[10]. Furthermore, the altered levels of transcripts from genes influenced by transcription factors known to be regulated by the Mediator complex and CDK8/19 are consistent with our compounds affecting CDK8/19-regulated gene transcription beyond WNT signalling (Supplementary data sets 1 and 3)[35,36].

Confirmation of cell-based target engagement by CCT251545

In our microarray profiling experiments we detected changes in transcript levels likely to result from changes to STAT-regulated signalling (Supplementary data set 1), consistent with a recent report[32] of CDK8-mediated phosphorylation of STAT1 (signal transducer and activator of transcription 1) at $STAT1^{SER727}$. Given these observations, we explored the effect of **1** on $STAT1^{SER727}$ phosphorylation in cells. Pleasingly, we demonstrated potent time- and concentration-dependent reduction of phospho-$STAT^{SER727}$ levels in the three human colorectal cancer cell lines used earlier (COLO205, LS174T and SW620). When tested at a concentration 10 times its IC_{50} in the respective cell-based reporter assay, **1** reduced phosphorylation at $STAT1^{SER727}$ within 10 to 20 minutes of treatment, with sustained inhibition at 6 and 24 hours. In addition, at 6 and 24 hours, **1** reduced phospho-$STAT1^{SER727}$ levels at concentrations consistent with those that reduced WNT-reporter activity in the same cell lines (Fig. 6a).

CDK8 has been reported to regulate the basal transcriptional machinery through phosphorylation of the carboxy-terminal domain (CTD) of RNA polymerase II ($POLR2A^{SER2}$ and $POLR2A^{SER5}$)[37] and also to phosphorylate $E2F1^{SER375}$, inhibiting its repressive activity towards β-catenin[38]. We did detect decreased $POLR2A^{SER2/5}$ phosphorylation following treatment of SW620 cells with **1**, although total POLR2A was also decreased to a comparable extent. In the same experiment $STAT1^{SER727}$ phosphorylation was potently reduced by **1**, but not the inactive analog **7**; importantly, total STAT1 levels were unaffected. We did not detect reduced $E2F1^{SER375}$ phosphorylation following treatment of SW620 cells with a high concentration of **1** that did inhibit phospho-$STAT1^{SER727}$ in the same samples (Supplementary Fig. 10**)**. Thus, of the three reported substrates of CDK8 tested in our models, we found phosphorylation of $STAT1^{SER727}$ to be the most robust and reliable target engagement biomarker of CDK8 inhibition by **1**.

Interestingly, we did not observe significant modulation of phospho-$STAT1^{SER727}$ levels in SW620 cells treated with sorafenib, ponatinib or linifanib at concentrations where treatment with **1** does lead to a significant reduction in phosphorylation, as measured both by bead-based ELISA and immunoblotting (Fig. 6b and Supplementary Fig. 11**)**. Indeed, ponatinib

and linifanib are significantly less potent than **1** (phospho-STAT1^{SER727} IC_{50} = 2800, 1800 and 9 nM respectively), whilst sorafenib had a minimal effect even at the highest concentration tested (10 μM). These observations are consistent with our earlier suggestion that Type II inhibitors of CDK8/19, including ponatinib, are less able to engage these kinases in the cellular context.

In vivo activity of CCT251545 in animal models

To assess the *in vivo* activity of **1**, we developed an animal model of intestinal hyperplasia dependent upon the expression of a dox-inducible mutant β-catenin transgene[29]. Oral dosing of **1** for 2 days (75, 37.5 and 18.75 mg/kg bid) dose-dependently reduced the length of hyperplastic crypts with the maximum effect similar to the removal of dox. We observed a concomitant reduction in proliferation and increased cell differentiation in goblet cells as quantified by BrdU and Alcian Blue staining respectively (Fig. 6c). We also detected a WNT gene expression signature (Supplementary Fig. 12**)** consistent with that observed for **2** in murine β-catenin dependent intestinal organoids (Fig 5a) and also for **2** and **6** when tested *in vivo* in the same model of intestinal hyperplasia bearing a dox-inducible mutant β-catenin transgene (Supplementary Fig. 13 and 14). Taken together, this data substantiate the pharmacological equivalence of compounds **1**, **2** and **6**.

The above reversal by our compounds of intestinal hyperplasia phenotypes induced by mutant β-catenin prompted us to examine the response to **1** in two different WNT-dependent tumor models. Firstly, in MMTV-WNT1-induced murine breast cancer allografts transplanted into athymic mice treatment with **1** (75 and 37.5 mg/kg qd or bid respectively) caused a decrease in tumor growth rate (Fig. 6d and 6e). We also detected concomitant reduction in the expression of the WNT target genes *Axin2* and *Lbh*, and induction of *Igfbp5*, a negatively-regulated target of the WNT pathway whose expression is associated with tumor regression[39,40]. Altered expression of all three genes was significant by Kruskal-Wallis non-parametric ANOVA test ($p<0.05$), although only decreased expression of *Igfbp5* retained significance ($p<0.05$) when corrected for multiple testing using Dunn's post-hoc test (Fig. 6f). In addition, compound **1** inhibited the growth of *APC*-mutant SW620 human colorectal cancer cells (GI_{50} = 140 nM; Supplementary Fig. 15**)** and treatment athymic mice bearing established SW620 human colorectal cancer xenografts with **1** (70mg/kg bid for 14 days) caused an ibition of tumor growth with a 70% reduction in final tumor weight relative to control (Supplementary Fig. 15**)**. We also observed a concomitant reduction in phospho-STAT1^{SER727} in tumor tissue (Supplementary Fig. 15**)**. Plasma and tumor concentrations of **1** were measured at 2 hours (2525±921 nM and 1598±324 nM respectively) and at 6 hours (188±64 nM and 639±115 nM respectively) after the last dose, demonstrating exposures above the cell-based GI_{50} at these time points.

DISCUSSION

CDK8 resides on a region of chromosome 13 known to undergo a gain of gene copy number in ~60% of colorectal cancers and inducible shRNA-mediated knockdown of CDK8 reduces the growth of HT29 and Colo205 human colorectal cancer tumor xenografts that harbor an amplified CDK8 gene[41]. In addition, CDK8 expression transforms NIH3T3 cells whereas a

kinase-dead mutant does not, consistent with its putative kinase-dependent role as an oncogene[28]. CDK8 expression is also reported to correlate with β-catenin activation in colon and gastric cancers and with increased mortality in colorectal, breast and ovarian cancers[42-44]; it is also reportedly overexpressed and essential for cell proliferation in melanoma[45]. These various results, incorporating use of RNAi and other biological perturbation, are consistent with CDK8 acting as a kinase-dependent driver oncogene in these settings and point to the need for high quality chemical probes[46-48] to further explore the biological roles of CDK8/19 in various biological and pathological contexts, as well as to uncover the potential utility of small molecule CDK8/19 inhibitors for the treatment of cancer and other human diseases.

Cortistatin A[49] was the first-reported ligand for CDK8/19 and recent patent disclosures signpost an emerging interest in CDK8 inhibitors[50,51]. A co-crystal structure of the Type II kinase inhibitor sorafenib with CDK8/cyclin C has been reported[22] and subsequent elegant studies examined the binding kinetics of fragment-like CDK8 ligands[52].

Here we demonstrate that the 3,4,5-trisubstituted pyridine CCT251545 (**1**) has the attributes of a potent and selective chemical probe for CDK8/19. Supported by a range of other evidence provided here, the identification of CDK8 and CDK19 as well as their cognate Mediator complex partners, as the only proteins from cell lysates that bind with high avidity to an affinity matrix comprising the close analog **5** provides strong evidence to reinforce the selective binding of this compound class in the cellular context. Protein X-ray crystallography studies of **1** in complex with CDK8/cyclin C reveal an unusual protein binding conformation which may explain the observed kinase selectivity and enable the design of alternative CDK8/19-selective scaffolds. These studies provide a further example of potent and selective kinase inhibition via a Type 1 binding mode.[53]

In contrast to Type II inhibitors tested here, compound **1** displays good translation to cell-based activity, including inhibition of $STAT1^{SER727}$ phosphorylation as a useful target engagement and pharmacodynamic biomarker of CDK8 inhibition. Furthermore, compound **1** modulates WNT-dependent gene mRNA abundance in several *in vitro* cell models and in murine β-catenin dependent intestinal organoids; thus it broadly phenocopies the changes seen in levels of selected transcripts following inhibition of WNT signalling by loss of activated β-catenin, consistent with our previous report that the 3,4,5-trisubstituted pyridine series acts at the TCF locale[10]. Also, while these compounds are not general transcriptional modulators, they clearly demonstrate both positive and negative effects on gene transcription that extend beyond WNT signalling and are related to additional on-target effects of modulating CDK8/19 Compound **1** inhibits the growth of MMTV-WNT1 breast cancers transplanted from genetically engineered mice as well as *APC*-mutant SW620 human colorectal cancer xenografts where we also demonstrate CDK8 target engagement through concomitant reduction in levels of phospho-$STAT^{SER727}$ and thereby establishing a link between CDK8 inhibition and WNT pathway modulation in the *in vivo* context. While these initial data appear promising, the effects of **1** across multiple CDK8/19-regulated pathways indicate that more extensive pharmacology studies and safety profile characterisation will be required to substantiate whether potent and selective CDK8/19 inhibitors have potential as therapeutics for the treatment of cancer and other human diseases. Given the role of WNT

signalling in stem cell biology, it will also be of interest to assess the impact of CDK8/19 inhibitors on the fate of cancer stem cells.

ONLINE METHODS

SILAC assay for target identification

Carried out by Evotec AG, Munich, Am Klopferspitz 19a, 82152 Martinsried, Germany[18]. LS174T-L5 cells, a derivative of LS174T cells that have been transduced with a TCF/LEF reporter construct[10] were grown in medium containing either arginine and lysine (Light) or heavier isotopic variants of these amino acids (Medium and Heavy). Proteins captured from the cell lysates by inhibitor-coupled sepharose beads were eluted, subjected to tryptic digestion and analysed by quantitative mass spectrometry.

Crystal structure of CDK8/cyclin C in complex with CCT251545 (pdb code: 5BNJ)

Human CDK8/cyclin C complex was expressed, purified and crystallised as described previously[22,44]. Protein at a concentration of 11.3 mg/ml was crystallised at 20°C by hanging drop vapour diffusion against 20 % PEG 3350 and 0.2 M sodium formate. Crystals were back-soaked and assessed for different time periods within intervals from 5 min up to 24 h within a concentration range of 0.2 - 2 mM ligand and shock-frozen with 25 % ethylene glycol as cryoprotectant. The best crystal used for structure determination belonged to the orthorhombic space group $P2_12_12_1$ with cell constants of a = 70.78 Å, b = 71.49 Å, c = 172.54 Å and $\alpha = \beta = \gamma = 90°$. X-ray diffraction data were collected on X06SA-PX beamline at Swiss Light Source synchrotron radiation source using Pilatus detector and the images were indexed, integrated and scaled using XDS and XSCALE program packages. The structure was solved by molecular replacement using the program MOLREP from the CCP4 program suite with a previous solved model. Subsequently, several cycles of refinement using the program REFMAC and crystallographic model building using the graphic package COOT were applied. Water molecules were built at stereochemically reasonable sites. For crystallographic data and refinement statistics see Supplementary Table 11**,** for an Fo-Fc omit map at 2.5 σ cutoff see Supplementary Fig. 16.

CDK8/cyclin C and CDK19/cyclin C reporter displacement assay

Binding kinetics were determined using a reporter displacement assay. In brief, the assay is based upon the competitive displacement of a reporter probe designed to selectively target the ATP binding site of CDK8 or CDK19 with a fast binding kinetic signature. Binding of the probe to its target results in the emission of an optical signal. Competitive displacement of the probe by the corresponding compounds results in a loss of the optical signal that can be quantified with increasing compound concentrations. IC_{50} values and kinetic parameters of the tested inhibitors were determined as described previously[54].

Protein expression and purification

CDK8/cyclin C complex was purchased from Proteros Biostructures. Human CDK8 (1-464) and human cyclin C (1-283) were separately expressed in insect cells and purified by affinity and size exclusion chromatography (SEC). The complex was formed *in vitro* and further purified by SEC. A tool compound which binds to the CDK8 ATP-site, was added to

Europe PMC Funders Author Manuscripts

stabilise the complex upon proteolytic removal of the GST fusion tag. In the final purified complex cyclin C is fused to an S-tag.

SPR protocol

CDK8/cyclin C protein complex was immobilised onto CM5 (series S) sensor chips using standard amine coupling. HBS-N, which consisted of 10 mM Hepes pH 7.4, 0.15 M NaCl, was used as a running buffer. The carboxymethyldextran surface within one side of the flow cell was activated with a 7 min injection of a 1:1 ratio of 0.4 M EDC and 0.1 M NHS. CDK8/cyclin C protein complex was diluted in 10 mM BisTris, pH 6.5 with 2μM staurosporine to a concentration of 10 μg/mL. The enzyme was coupled to the surface with a 1 - 3 min injection at a flow rate of 10 μL/min. Remaining activated groups were blocked with a 7 min injection of 1.0 M ethanolamine, pH 8.5. Typically 3000 ± 1000 RU's of CDK8/cyclin C protein complex was immobilised. Compounds (stored as 10 mM stock solutions in 100% dimethyl sulfoxide (DMSO)) were dissolved directly in running buffer (20 mM HEPES, pH 7.4, 150 mM NaCl, 5 mM $MgCl_2$, 1 mM DTT, 0.05% P20, 0.1 mM EGTA, 2% DMSO) and analyzed with a Biacore S51 using a 2-fold dilution series. The highest compound concentration varied according to the expected dissociation constant and all compounds were tested at 10 different concentrations, each concentration was tested at least three times. Interaction analysis cycles consisted of a 120 s sample injection (30 μL/min) followed by 350 s of buffer flow (dissociation phase). All sensorgrams were processed by first subtracting the binding response recorded from the control surface (reference spot), followed by subtracting an average of the buffer blank injections from the reaction spot. To determine kinetic rate constants, all data sets were fitted to a simple 1:1 interaction model including a term for mass transport using numerical integration and nonlinear curve fitting. Equilibrium analysis was performed by fitting the response at the end of the association phase to a single-site binding isotherm.

Cell and Organoid Culture

All cells used in this study were obtained from ATCC (LGC Promochem), were confirmed to be mycoplasma free using a Mycoplasma detection kit (Lonza, LT017-710) and were authenticated by short tandem repeat profiling. Cells were propagated at 37°C in a humidified incubator with 5% CO_2 in air using Dulbecco's Modified Eagle's Medium without phenol red (Gibco #41966) and supplemented with 10% v/v foetal bovine serum (Biosera cat. # F1830), 2% v/v L-glutamine (GIBCO cat. # 25030) and 1% v/v non-essential amino acids (GIBCO cat. # 11146) and sub-cultured when they reached 80% confluence. Tet-O-β-catenin intestinal organoid culture and RNA extraction was carried out as previously described[29].

CETSA (cellular thermal shift assay) analysis

SW620 cells were incubated for 2 hours with indicated concentrations (30, 3, 0.3, 0.03 and 0.003 μM) of compound **1**, sorafenib, linifanib or ponatinib. Control cells were treated with 0.3% DMSO. Cells were lysed in lysis buffer (50 mM Tris-HCl pH 7.4, 150 mM NaCl, 1% Triton X-100, 1 mM EDTA, 20 mM β-Glycerolphosphate, 1% Phosphatase-Inhibitor Cocktail Set II (Calbiochem, Cat. #524625), 0.1% Protease-Inhibitor Cocktail Set III

(Calbiochem, Cat. #539134), 0.01% Benzonase (Novagen, Cat. #70664)) and each lysate was split into two aliquots. One aliquot was kept at 4°C and the other aliquot was heated at 50°C for 3 min followed by cooling at room temperature for 3 minutes. After centrifugation (4°C, 16,000 × g, 20 min) CDK8/19 levels were determined in supernatants using a bead-based ELISA.

Immunoblotting analysis of protein expression

Cells (2 mL) were plated into 6-well plates at a density of 1×10^5 cells/ mL and were incubated in a humidified tissue culture incubator for 24 h at 37°C and 5% CO_2. DMSO-dissolved test compounds were added to the wells at specific concentrations and incubated for 6 hours, after which cells were lysed with RIPA buffer on ice, frozen at −80°C overnight and probe-sonicated for complete extraction of nuclear and cytoplasmic proteins. The lysates were centrifuged at 13,000 rpm for 15 minutes and proteins harvested in the supernatant and protein concentration measured using the BCA assay. 20 μg of protein was added to 2 x loading buffer and boiled for 5 minutes at 95°C. Samples were resolved on SDS-4-12%PAGE gels. After transfer to nitrocellulose membranes, blots were blocked at room temperature for 1 h in 5% BSA in TBS-T (0.1% Tween 20, 50 mM Tris-Cl, pH 7.6, 150 mM NaCl) and incubated at 4°C overnight with antibodies specific for phospho-STAT1^{SER727} (Cell Signaling, #8826), total STAT1 (Santa-Cruz, #346), GAPDH (Merck Millipore, MAB374), Phospho-POLR2A^{SER2} (#A300-654A), Phospho-POLR2A^{SER5} (Bethyl Labs, #A300-655A) or total POLR2A (Bethyl Labs, #A300-653A). After washing with TBS-T, blots were incubated with HRP-conjugated secondary antibodies in blocking buffer at room temperature and bands were visualised using the enhanced chemoluminescence (ECL prime) method.

Generation of monoclonal rabbit antibodies against phospho-E2F1^{SER375}

A monoclonal rabbit antibody against phospho-E2F1^{SER375} was generated by Epitomics, Inc.. Briefly, rabbits were immunised with 5 boosts of the peptide NH2-RAPVDEDRL(pS)PLVAADSC conjugated to KLH. Antibody titer was monitored by ELISA using the same phosphopeptide used for the immunisation but conjugated to BSA. In addition, a phosphopeptide corresponding to the equivalent region in murine E2F1 (RVPMEEDQL(pS)PLVAADSC) and the unphosphorylated peptide of the human protein (RAPVDEDRLSPLVAADSC) were used for screening. Following the selection of the rabbit with the best signal in the ELISA, lymphocytes were isolated from its spleen und fusion was performed to obtain hybridomas. Multiclone hybridoma supernatants were screened by ELISA as above and hybridomas with the desired profile were further subcloned and re-screened to identify the final hybridoma clone. The cDNAs from the IgG heavy chain and light chain were amplified by PCR, sequenced, inserted into a mammalian expression vector and transiently expressed in HEK293 cells. Recombinant antibody was purified using a protein A column and then used in a bead-based ELISA together with commercially available antibodies against total E2F1 (sheep-anti-E2F-1, R&D Systems #AF4825 and rabbit-anti-E2F-1, Cell Signalling #3742) to quantify phospho-E2F1^{SER375} and total E2F1. Supplementary Fig. 11 shows the final validation of the total-E2F1 and phospho-E2F1^{SER375} reagents in cells co-expressing an inducible CDK8 and E2F1^{WT} or mutant E2F1^{S375A}/E2F1^{S375D}.

ShRNA Protocol

The human colon cancer cell line Colo205 was transduced with a lentivirus encoding a short half-life luciferase (with a destabilised PEST sequence construct; construct F1921): 16 x TCF/LEF transcription sites - short half-life firefly luciferase on a basal pTA promoter – hygromycin resistance gene on an EF-1-α promoter. This construct was made in-house using the lentiviral base vector: pCDH-CMV-MCS-EF1-Hygro from System Biosciences (cat. # CD515B-1). This generated the Colo205-F1921 subline expressing a luciferase with a half-life of about 60 minutes.

TRIPZ and GIPZ shRNA gene knockdown constructs for CDK8 (V2THS_112900, V2THS_112909, V2THS_112911) and CDK19 (V2LHS_77136, V3LHS_356652, V2LHS_202355) were purchased from Open Biosystems (GE Healthcare Dharmacon Inc) as bacterial glycerol stocks and plasmid DNA was extracted from an overnight culture using a Qiagen MiniPrep kit. Viral supernatant was produced by co-transfection of individual constructs with packaging plasmids into HEK293 cells and incubation for 48 h. The spun supernatant was tested for optimal titre with Lenti-X GoStix (Clontech Takara Bio). A supernatant cocktail that contained either all three CDK19 or CDK8 packaged constructs were used to spinnoculate sub confluent Colo205-F1921 cells and seeded into 6 well plates with the addition of Polybrene @ 8 μg/mL. After 48 h cells were trypsinised and reseeded into 175cm^3 tissue culture flasks containing 1μg/mL puromycin to select stable clones. After antibiotic selection for one week, the transduced Colo205-F1921 cells were FACS sorted for either GFP-positive, RFP-positive or GFP+RFP-positive cells and expanded in culture. For analysis of TCF-dependent transcriptional activity, 100 μL of cells were plated into 96-well plates (Corning 3917) at a density of 2×10^5 cells/mL and cultured for 24 h as described above. Cells were then lysed using 100 μL of Steady-Glo luciferase reagent (Promega, E2520) and luminescence read on a TopCount luminometer (Perkin Elmer) after 60 min incubation at ambient temperature in a semi-dark room.

esiRNA Protocol

Pools of esiRNA targeted against CDK8, CDK19, β-catenin, APC and Renilla luciferase (control) mRNA were obtained from Sigma (cat. # EHU023981, EHU061571, EHU139421, EHU079171 and EHUFLUC respectively). 10.0 ng of each esiRNA pool were pipetted into single wells of a white 384 well plate (Greiner M1437-32EA) and made up to 20 ng total per well if necessary with control esiRNA in a total volume of 5 μl in water. To this was added 0.28 μl/well Hiperfect siRNA transfection reagent (Qiagen 301705) made up to a total volume of 7 μl/well with OptiMEM (Invitrogen 31985-047). After complex formation (10 min), 6000 7dF3 WNT reporter cells[11] in 30 μl medium was pipetted into each well. After 24 hours of incubation at 37°C/5% CO_2, 5 μl of 40 μM oestradiol (Sigma E2257) in medium (diluted from a 2 mM stock in ethanol) was added to activate the Dvl2-ER fusion protein and induce WNT pathway activity. After a further 24 hours incubation, 50 μl BrightGLO luciferase substrate reagent (Promega E2620) was added to each well for 5 min. The resulting luminescence was then quantified on a Fluostar plate reader (BMG) in luminescence mode. The experiment was repeated 3 times.

CDK8 Overexpression

Constructs coding for mycCDK8wt and its kinase-dead (D173A) mutant were inserted into the FRT site of previously-described T-Rex HEK293 Tet-O cells (Life Technologies) that have the TCF-firefly luciferase-IRES- GFP (TLIG) reporter [10]. The cells were maintained in culture in DMEM with high glucose supplemented with GlutaMAX, Pen/Strep, 12μg/ml Blasticidin and 300μg/ml Hygromycin (Life Technologies). For the luciferase assay, cells were seeded at 30,000 cells/well into a 96-well plate in 80μL medium. 24 hours later, the cells were treated with 0.05μg/ml Doxycycline in H2O or H2O alone (4 wells per treatment). After 24 hours, the medium was removed and the cells were lysed in 50μL/well Glo lysis buffer (Promega) with agitation for 5 minutes. 50μL Bright Glo reagent (Promega) was then added to each well and the luciferase intensities were read using a BMG FLUOstar Optima plate reader in luminescence mode. For the Western Blot, cells were seeded at 900,000 cells per well of a 6-well dish in 2ml medium and treated as shown above, at the same time. Cells were harvested in RIPA buffer, separated by SDS gel-electrophoresis and probed with antibodies to CDK8 and β-tubulin (Cell Signalling 4196S and 2146S respectively). The experiment was repeated 4 times.

qRT-PCR

RT reactions were carried out on 300-1,000 ng RNA with the Improm II kit (Promega) according to the manufacturer's instructions. The PCR reactions were performed in the Sensimix Sybr green 2x mastermix (Bioline) on an Opticon Chromo II qPCR machine using 40 cycles of 95°C for 15s, 55°C for 15s and 72°C for 15s. Relative expression values were calculated using the $\Delta\Delta C_T$ method[55]. The significance was determined with Kruskal-Wallis non-parametric ANOVA and Dunn's post-hoc tests. Details of primers used for qRT-PCR can be found in Supplementary Table 12.

Tet-O-Δ1-89-β-Catenin mouse studies

Cohorts of eight, randomly-allocated mice were used for each treatment. The drinking water was supplemented with 2 mg/ml doxycycline (Sigma) and 10 mg/ml sucrose for 6-9 days to induce the hyperplastic small-intestine crypt phenotype. Doxycyline was withdrawn for the 'Dox Removal' cohort but was continued for the remainder. In addition, it was necessary to supplement this with an intraperitoneal injection (i.p.) of 2 mg/ml doxycycline in PBS (1% W/V) to maintain levels. The latter was given concurrently with vehicle alone, (10% DMSO/5% Tween 20/85% 0.9% NaCl) or vehicle + 100 mg/kg **2** given 3 times over 24 hrs by oral gavage. RNA extraction was carried out from 3 mm sections of the anterior duodenum (stored in RNAlater (Sigma) at 4°C overnight) as previously described[34]. qRT-PCR was performed as described above. For dose-dependent experiments, 18.75, 37.5 and 75 mg/kg **1, 6** or vehicle was orally gavaged bi-daily for 2 days as above and BrdU (Sigma) at 2 mg/ml in PBS was injected i.p. 2 hours prior to euthanasia.

Gene-Expression Microarray

Total RNA was also analysed by microarray expression profiling. Organoid or cell line total RNA was labelled with Cye3-CTP and a mouse or human reference standard RNA (Stratagene) was labelled with Cye5-CTP by direct incorporation using a Quick-Amp

labeling kit (Agilent). Purified, labelled cDNA products were hybridised to 8 × 60K mouse or human microarray following the manufacturers' instructions (Agilent). Microrarray slides were washed, scanned and analysed. Mouse organoid data were analysed using Arraytools (http://linus.nci.nih.gov/BRB-ArrayTools.html) and the colon cancer cell line data using Genespring (Agilent). A similar analysis was performed on both datasets. Lowess intensity dependent normalization was used to adjust for differences in labelling intensities of the Cy3 and Cy5 dyes[56]. We identified genes that were differentially expressed using a multivariate permutation test to provide confidence that the false discovery rate was less than 5%[56,57]. The test statistics used were random variance t-statistics for each gene[56]. Although t-statistics were used, the multivariate permutation test was non-parametric and does not require the assumption of Gaussian distributions. The significantly differentially expressed genes were investigated for enrichment in terms of particular pathways or potential transcription factor regulation using the Metacore software (Thomson Reuters). Microarray data are available on the NCBI Gene Expression Omnibus (GEO; http://www.ncbi.nlm.nih.gov/geo/) website under accession number GEO GSE67849.

Effect on crypt morphology by immunohistochemical staining

Duodenal segments from treated mice were fixed overnight in 10% (v/v) formaldehyde in PBS for 16 h at 4°C, embedded in paraffin by standard automated techniques and sectioned. Sections were deparaffinised in 3 changes of xylene and rehydrated through graded alcohols (2x 100%, 2x 95%, 1x 70% ethanol (v/v) in water). Subsequently, they were placed in 2N HCl for 30 min at 37°C, rinsed thoroughly in PBS and then treated for a further 20 min at 37°C with 100μl pre-warmed 0.05% trypsin in PBS (Invitrogen). The sections were then rinsed with PBS and blocked in 100μl blocking solution from the Mouse-On-Mouse immunostaining kit (Vector Labs) for 1 hr, followed by incubation with 1:1000 anti-BrdU mouse monoclonal antibody (clone BU-33, Sigma B8434) in MOM solution (from the Mouse-on-Mouse immunostaining kit from Vector Labs) overnight at 4°C. This was followed by treatment with the biotinylated secondary antibody and ABC solution from the Mouse-On-Mouse immunostaining kit (Vector Labs) according to the manufacturer's instructions. The sections were counterstained with Mayer's haematoxylin (Sigma) for 1 min, copiously washed in tap water and dehydrated though graded alcohols (1x 70%, 2x 95%, 2x 100% ethanol (v/v) in water) and 3 changes of xylene. The sections were then mounted in DPX (Sigma). Sections for Alcian Blue staining to detect the goblet cells were processed according to the method previously described[58]. Crypt length, % BrdU positive cells and % goblet cells were counted in 50 crypts according to the half-crypt scoring system previously described[59]. The Kruskal-Wallis non-parametric ANOVA with Dunn's post-hoc tests was used to determine the significance of the results.

MMTV-WNT-1 allograft transplant model

MMTV-WNT-1 allograft tissue from immunocompromised mice[40] was chopped into fragments of <1 mm^3 and transplanted using a trochar into the flanks of CD1 (*Nu/Nu*) mice that had been transiently anaesthetised with isofluorane. Once the tumours had grown to > 5mm^3, the animals were randomly assigned to three cohorts of 8 to be orally gavaged with vehicle (10% DMSO/5% Tween 20/85% 0.9% NaCl), 37.5 mg/kg or 75 mg/kg **1**, bi-daily for 10 days. Tumour dimensions were measured daily using a caliper. Tumour volume in

mm^3 was calculated using the formula: volume = ($width^2$ × length)/2. Tumour tissue samples for RNA extraction were stored in RNAlater (Sigma) at 4°C overnight and RNA isolation was carried out as previously described[29].

SW620 3D Clonogenic Assay

The assay was performed in 96 well format according to a modified two-layer soft agar assay[60]. Each test well contained three layers of equal volume: 2 layers of semi-solid medium (bottom and top layer), and one layer of medium supernatant, with or without test compound. The bottom layer consisted of 0.1 mL/well MEM Alpha Medium (supplemented with 10% (v/v) fetal calf serum, sodium bicarbonate, penicillin-streptomycin (Pen Strep), L-glutamine, sodium pyruvate and 1% (w/v) agar). 4×10^3 Cells were added to 0.1 mL of the same culture medium supplemented with 0.7% (w/v) agar and plated in onto the bottom layer. Compound **1** was added after serial dilution in DMSO and transfer in cell culture medium, and left on the cells for the duration of the experiment (continuous exposure, 0.03 mL drug overlay). Each plate included six untreated control wells and drug treated groups in quadruplicate at 15 concentrations (compound concentration range from 30 μM to 10 pM). Cultures were incubated at 37°C and 10% CO_2 in a humidified atmosphere for 14 days. Viability of tumor cells in soft-agar culture was determined by Alamar Blue staining. The full dose-response curve from four technical repeats is shown in Supplementary Figure 15.

SW620 human tumour xenograft model

Three million SW620 human colorectal carcinoma cells were injected s.c. in the right flanks of female NCr athymic mice 6-8 weeks of age. Therapy was initiated when established tumours reached a mean volume of 60mm (day 13). Animals were randomly assigned to two cohorts of 10. Control mice received vehicle (10% DMSO, 5% Tween 20, 85% saline) and treated animals compound **1** at 70mg/kg orally twice daily with a 2-day break after one week's dosing. Tumours volumes and body weights were measured three times weekly and the study was terminated on day 14. Plasma and tumour samples were collected for pharmacokinetic and pharmacodynamic biomarker analysis.

Pharmacokinetic Analysis

Plasma and tumour homogenates were extracted with 3 equivalent volumes of methanol containing olomoucine (500nM) as an internal standard. Extracts were quantified for compound **1** using an external calibration method (8 point calibration curve with 4 quality control samples) by multiple reaction monitoring on an Agilent 6410 triple quadrupole mass spectrometer following chromatographic separation using a Phenomenex Kinetex C 18 HPLC column (2.6um, 50mmX2.1mm ID) with a 5 minute linear gradient 90/10 to 10/90 0.1% formic acid/methanol on an Agilent 1290 LC system.

Phospho-STAT1^{SER727} protocol

Tumours were excised, immediately snap-frozen in liquid nitrogen and stored at −80°C. Samples were later transferred to MK28 reinforced homogenising tubes with metal beads (Stretton Scientific) lysis buffer and phosphatase inhibitors (Sigma P5726 and P0044 1:50 dilution) added immediately. The samples were ground using a Precellys 24 at 6000rpm, 2x

20sec (Stretton Scientific). Tumour lysates were frozen at −80°C, thawed, sonicated in a water bath for 3 min, then incubated on ice for 10 min. Tubes were spun at 14000rpm at 4°C for 10 min and supernatants were collected, aliquoted and frozen at −80°C until analysis. Tumour lysates were diluted 1:5 in lysis buffer and the concentrations determined using a Direct Detect® spectrometer (Merck Millipore). Samples were aliquoted, then boiled in electrophoresis sample buffer and loaded on SDS-4-12%PAGE gels. After transfer to PVDF membranes, blots were blocked at room temperature for 1 h in blocking buffer (5% dry milk in TNT: 1M Tris HCL pH8, 5M NaCl, 0.1% Tween 20) and incubated at 4°C overnight with 1:1000 rabbit anti-STAT1 (Santa Cruz, sc-346), 1:2000 rabbit anti p-STAT1^{SER727} (Cell Signalling Technology, #8826) or 1:10000 mouse anti-GAPDH (Abcam, Ab-8245) antibodies. After washing with TNT, blots were incubated with HRP-conjugated secondary antibodies in blocking buffer at room temperature and bands were visualised using the enhanced chemoluminescence (ECL prime) method.

All animal studies were conducted in accordance with guidelines for the welfare and use of animals in cancer research[61]. We comply with the NCRI Guidelines and all work is approved by our own institutional Ethics Committee and the UK Government's Home Office.

Supplementary Material

Refer to Web version on PubMed Central for supplementary material.

Acknowledgements

This work was supported by Cancer Research UK [grant number C309/A11566]. We acknowledge Cancer Research UK funding to Cancer Research UK Centre at The Institute of Cancer Research and The Royal Marsden NHS funding to the NIHR Biomedical Research Centre at the same institutions. We thank Dr Amin Mirza, Mr Meirion Richards and Dr Maggie Liu for their assistance with NMR, mass spectrometry and HPLC. We thank Stefanie Gaus (Merck Serono) for excellent technical assistance. We thank the team of Proteros Biostructures GmbH, Bunsenstrasse 7a, D-82152 Martinsried, Germany for the Reporter Displacement Assay and in particular E. V. Schneider and A. Lammens for the X-ray co-crystal structure of CCT251545 with CDK8/cyclin C.

REFERENCES

1. Eggert US. The why and how of phenotypic small-molecule screens. Nature chemical Biology. 2013; 9:206–209. [PubMed: 23508174]
2. Blagg J, Workman P. Chemical biology approaches to target validation in cancer. Current Opinion in Pharmacology. 2014; 17:87–100. [PubMed: 25175311]
3. Bunnage ME. New Frontiers in Chemical Biology, Enabling Drug Discovery. 2011; 43
4. Bantscheff M, Drewes G. Chemoproteomic approaches to drug target identification and drug profiling. Bioorganic & Medicinal Chemistry. 2012; 20:1973–1978. [PubMed: 22130419]
5. Ong SE, et al. Identifying the proteins to which small-molecule probes and drugs bind in cells. Proceedings of the National Academy of Sciences of the United States of America. 2009; 106:4617–4622. [PubMed: 19255428]
6. Swinney DC, Anthony J. How were new medicines discovered? Nature reviews. Drug Discovery. 2011; 10:507–519.
7. Huang SM, et al. Tankyrase inhibition stabilizes axin and antagonizes Wnt signalling. Nature. 2009; 461:614–620. [PubMed: 19759537]

8. Liu J, et al. Targeting Wnt-driven cancer through the inhibition of Porcupine by LGK974. Proceedings of the National Academy of Sciences of the United States of America. 2013; 110:20224–20229. [PubMed: 24277854]
9. Kahn M. Can we safely target the WNT pathway? Nature Reviews. Drug Discovery. 2014; 13:513–532. [PubMed: 24981364]
10. Mallinger A, et al. Discovery of Potent, Orally Bioavailable, Small-Molecule Inhibitors of WNT Signaling from a Cell-Based Pathway Screen. Journal of Medicinal Chemistry. 2015; 58:1717–1735. [PubMed: 25680029]
11. Clevers H. Wnt/beta-catenin signaling in development and disease. Cell. 2006; 127:469–480. [PubMed: 17081971]
12. Angers S, Moon RT. Proximal events in Wnt signal transduction. Nature Reviews. Molecular Cell Biology. 2009; 10:468–477. [PubMed: 19536106]
13. Carlsten JO, Zhu X, Gustafsson CM. The multitalented Mediator complex. Trends in Biochemical Sciences. 2013; 38:531–537. [PubMed: 24074826]
14. Kim S, Xu X, Hecht A, Boyer TG. Mediator is a transducer of Wnt/beta-catenin signaling. The Journal of Biological Chemistry. 2006; 281:14066–14075. [PubMed: 16565090]
15. Allen BL, Taatjes DJ. The Mediator complex: a central integrator of transcription. Nature Reviews Molecular Cell Biology. 2015; 16:155–166. [PubMed: 25693131]
16. Schiano C, Casamassimi A, Vietri MT, Rienzo M, Napoli C. The roles of mediator complex in cardiovascular diseases. Biochim. Biophys. Acta. 2014; 1839:444–451. [PubMed: 24751643]
17. Schiano C, et al. Involvement of Mediator complex in malignancy. Biochimica et Biophysica Acta. 2014; 1845:66–83. [PubMed: 24342527]
18. Sharma K, et al. Proteomics strategy for quantitative protein interaction profiling in cell extracts. Nature Methods. 2009; 6:741–744. [PubMed: 19749761]
19. Nemet J, Jelicic B, Rubelj I, Sopta M. The two faces of Cdk8, a positive/negative regulator of transcription. Biochimie. 2014; 97:22–27. [PubMed: 24139904]
20. Conaway RC, Conaway JW. Function and regulation of the Mediator complex. Current Opinion in Genetics & Development. 2011; 21:225–230. [PubMed: 21330129]
21. Martinez Molina D, et al. Monitoring drug target engagement in cells and tissues using the cellular thermal shift assay. Science (New York, N.Y.). 2013; 341:84–87.
22. Schneider EV, et al. The structure of CDK8/CycC implicates specificity in the CDK/cyclin family and reveals interaction with a deep pocket binder. Journal of Molecular Biology. 2011; 412:251–266. [PubMed: 21806996]
23. Lipton JH, et al. Comparative efficacy of tyrosine kinase inhibitor treatments in the third-line setting, for chronic-phase chronic myelogenous leukemia after failure of second-generation tyrosine kinase inhibitors. Leukemia Research. 2015; 39:58–64. [PubMed: 25466286]
24. Cainap C, et al. Linifanib Versus Sorafenib in Patients With Advanced Hepatocellular Carcinoma: Results of a Randomized Phase III Trial. Journal of Clinical Oncology. 2015; 33:172–179. [PubMed: 25488963]
25. Gozgit JM, et al. Ponatinib (AP24534), a multitargeted pan-FGFR inhibitor with activity in multiple FGFR-amplified or mutated cancer models. Molecular Cancer Therapeutics. 2012; 11:690–699. [PubMed: 22238366]
26. Shankar DB, et al. ABT-869, a multitargeted receptor tyrosine kinase inhibitor: inhibition of FLT3 phosphorylation and signaling in acute myeloid leukemia. Blood. 2007; 109:3400–3408. [PubMed: 17209055]
27. Garuti L, Roberti M, Bottegoni G. Non-ATP competitive protein kinase inhibitors. Current Medicinal Chemistry. 2010; 17:2804–2821. [PubMed: 20586715]
28. Firestein R, et al. CDK8 is a colorectal cancer oncogene that regulates beta-catenin activity. Nature. 2008; 455:547–551. [PubMed: 18794900]
29. Jarde T, et al. In vivo and in vitro models for the therapeutic targeting of Wnt signaling using a Tet-ODeltaN89beta-catenin system. Oncogene. 2013; 32:883–893. [PubMed: 22469981]

30. Krasley E, Cooper KF, Mallory MJ, Dunbrack R, Strich R. Regulation of the oxidative stress response through Slt2p-dependent destruction of cyclin C in Saccharomyces cerevisiae. Genetics. 2006; 172:1477–1486. [PubMed: 16387872]
31. Mokry M, et al. Integrated genome-wide analysis of transcription factor occupancy, RNA polymerase II binding and steady-state RNA levels identify differentially regulated functional gene classes. Nucleic Acids Research. 2012; 40:148–158. [PubMed: 21914722]
32. Bancerek J, et al. CDK8 kinase phosphorylates transcription factor STAT1 to selectively regulate the interferon response. Immunity. 2013; 38:250–262. [PubMed: 23352233]
33. Galbraith MD, et al. HIF1A employs CDK8-mediator to stimulate RNAPII elongation in response to hypoxia. Cell. 2013; 153:1327–1339. [PubMed: 23746844]
34. Donner AJ, Ebmeier CC, Taatjes DJ, Espinosa JM. CDK8 is a positive regulator of transcriptional elongation within the serum response network. Nature Structural & Molecular Biology. 2010; 17:194–201.
35. Galbraith MD, Donner AJ, Espinosa JM. CDK8: a positive regulator of transcription. Transcription. 2010; 1:4–12. [PubMed: 21327159]
36. Alarcon C, et al. Nuclear CDKs drive Smad transcriptional activation and turnover in BMP and TGF-beta pathways. Cell. 2009; 139:757–769. [PubMed: 19914168]
37. Rickert P, Seghezzi W, Shanahan F, Cho H, Lees E. Cyclin C/CDK8 is a novel CTD kinase associated with RNA polymerase II. Oncogene. 1996; 12:2631–2640. [PubMed: 8700522]
38. Morris EJ, et al. E2F1 represses beta-catenin transcription and is antagonized by both pRB and CDK8. Nature. 2008; 455:552–556. [PubMed: 18794899]
39. Rieger ME, Sims AH, Coats ER, Clarke RB, Briegel KJ. The embryonic transcription cofactor LBH is a direct target of the Wnt signaling pathway in epithelial development and in aggressive basal subtype breast cancers. Molecular and Cellular Biology. 2010; 30:4267–4279. [PubMed: 20606007]
40. Liu BY, et al. Mammary tumor regression elicited by Wnt signaling inhibitor requires IGFBP5. Cancer Research. 2012; 72:1568–1578. [PubMed: 22307840]
41. Adler AS, et al. CDK8 maintains tumor dedifferentiation and embryonic stem cell pluripotency. Cancer Research. 2012; 72:2129–2139. [PubMed: 22345154] Starr TK, et al. A transposon-based genetic screen in mice identifies genes altered in colorectal cancer. Science (New York, N.Y.). 2009; 323:1747–1750.
42. Firestein R, et al. CDK8 expression in 470 colorectal cancers in relation to beta-catenin activation, other molecular alterations and patient survival. International Journal of Cancer. 2010; 126:2863–2873. [PubMed: 19790197]
43. Kim MY, Han SI, Lim SC. Roles of cyclin-dependent kinase 8 and beta-catenin in the oncogenesis and progression of gastric adenocarcinoma. International Journal of Oncology. 2011; 38:1375–1383. [PubMed: 21344156]
44. Porter DC, et al. Cyclin-dependent kinase 8 mediates chemotherapy-induced tumor-promoting paracrine activities. Proceedings of the National Academy of Sciences of the United States of America. 2012; 109:13799–13804. [PubMed: 22869755]
45. Kapoor A, et al. The histone variant macroH2A suppresses melanoma progression through regulation of CDK8. Nature. 2010; 468:1105–1109. [PubMed: 21179167]
46. Bunnage ME, Chekler EL, Jones LH. Target validation using chemical probes. Nature Chemical Biology. 2013; 9:195–199. [PubMed: 23508172]
47. Frye SV. The art of the chemical probe. Nature Chemical Biology. 2010; 6:159–161. [PubMed: 20154659]
48. Workman P, Collins I. Probing the probes: fitness factors for small molecule tools. Chemistry & Biology. 2010; 17:561–577. [PubMed: 20609406]
49. Cee VJ, Chen DY, Lee MR, Nicolaou KC. Cortistatin A is a high-affinity ligand of protein kinases ROCK, CDK8, and CDK11. Angewandte Chemie. 2009; 48:8952–8957. [PubMed: 19844931]
50. Hu H, et al. Novel phenyl-piperidine/pyrazine amides for the treatment of cancer. 2014 WO2014029726.
51. Rzymski T, et al. Substituted tricyclic benzimidazoles as Kinase Inhibitors. 2014 WO2014072435.

52. Schneider EV, Bottcher J, Huber R, Maskos K, Neumann L. Structure-kinetic relationship study of CDK8/CycC specific compounds. Proceedings of the National Academy of Sciences of the United States of America. 2013; 110:8081–8086. [PubMed: 23630251]

53. Huang D, Zhou T, Lafleur K, Nevado C, Caflisch A. Kinase selectivity potential for inhibitors targeting the ATP binding site: a network analysis. Bioinformatics. 2010; 26:198–204. [PubMed: 19942586]

Online Methods References

54. Neumann L, von Konig K, Ullmann D. HTS reporter displacement assay for fragment screening and fragment evolution toward leads with optimized binding kinetics, binding selectivity, and thermodynamic signature. Methods in Enzymology. 2011; 493:299–320. [PubMed: 21371596]

55. Livak KJ, Schmittgen TD. Methods. 2001; 25:402–8. [PubMed: 11846609]

56. Simon, R., et al. Design and Analysis of DNA Microarray Investigations. Springer-Verlag; New York: 2003.

57. Korn EL, et al. Controlling the number of false discoveries: Application to high-dimensional genomic data. Journal of Statistical Planning and Inference. 2012; 75:447–60.

58. Sansom OJ, et al. Loss of Apc in vivo immediately perturbs Wnt signaling, differentiation, and migration. Genes & Development. 2004; 18:1385–1390. [PubMed: 15198980]

59. Li YQ, et al. Target cells for the cytotoxic effects of carcinogens in the murine small intestine. Carcinogenesis. 1992; 13:361–8. [PubMed: 1547525]

60. Hamburger AW, Salmon SE. Primary bioassay of human tumor stem cells. Science. 1977; 197:461–463. [PubMed: 560061]

61. Workman PW, et al. Guidelines for the welfare and use of animals in cancer research. British Journal of Cancer. 2010; 102:1555–1577. [PubMed: 20502460]

Europe PMC Funders Author Manuscripts

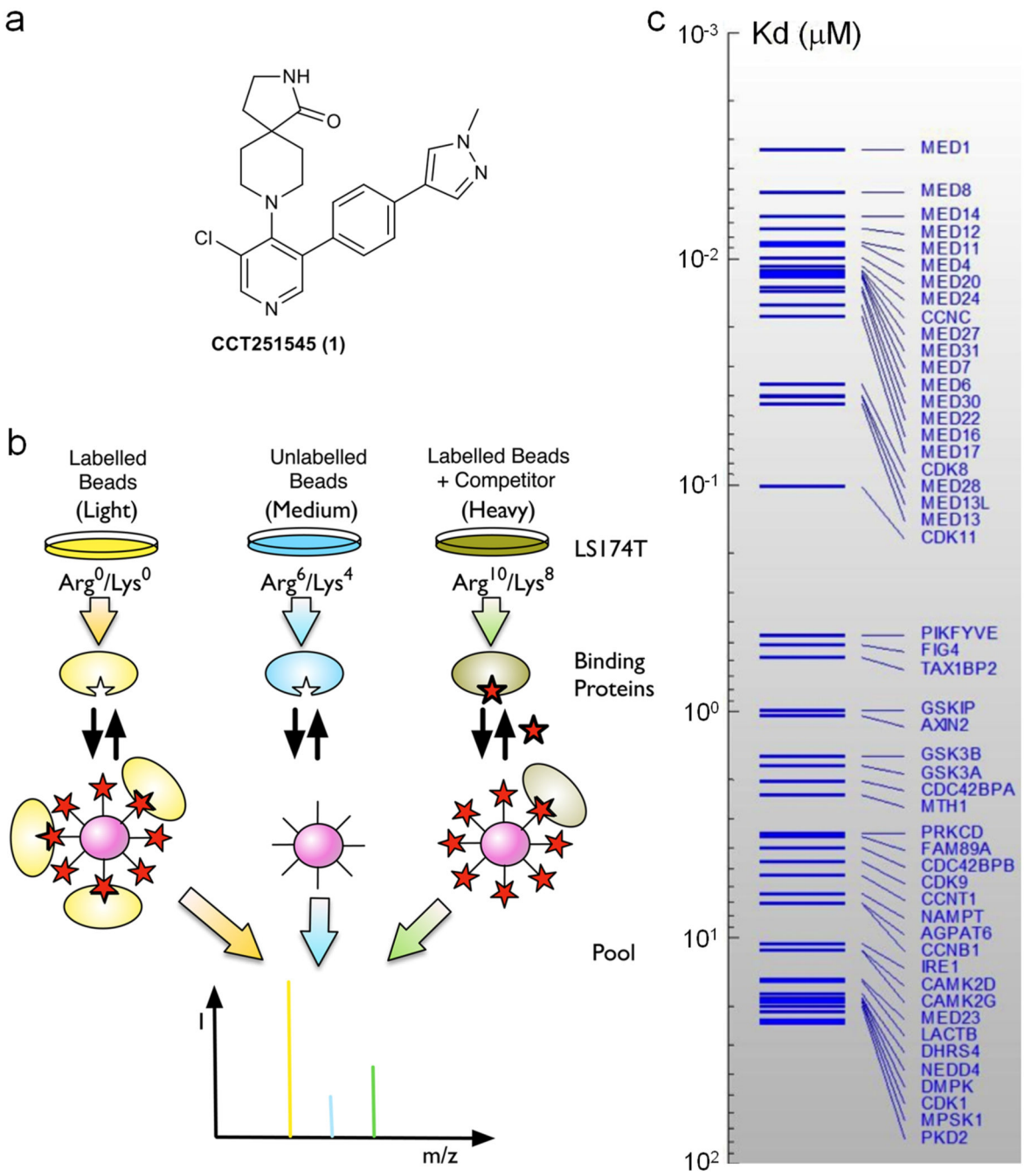

Figure 1. Identification of the molecular targets of CCT251545

a) Chemical structure of compound **1. b**) LS174T cells were SILAC-encoded with normal or stable isotope-labelled arginine and lysine. Cell lysates were incubated with control beads or beads coupled to **5** in the presence of 3 nM to 30 μM of **4**, **6**, or inactive control **7**. After washing, proteins that remained bound were eluted, separated by SDS-PAGE, trypsinised and analysed by LC-MS/MS. **c**) Ranked plot of proteins that selectively bound to compound **5** conjugated beads and were displaced by compound **4**, proteins are ranked according to

their affinities (K_d's in μM) from top to bottom. CDK19 is annotated as CDK11 in this Figure.

Europe PMC Funders Author Manuscripts

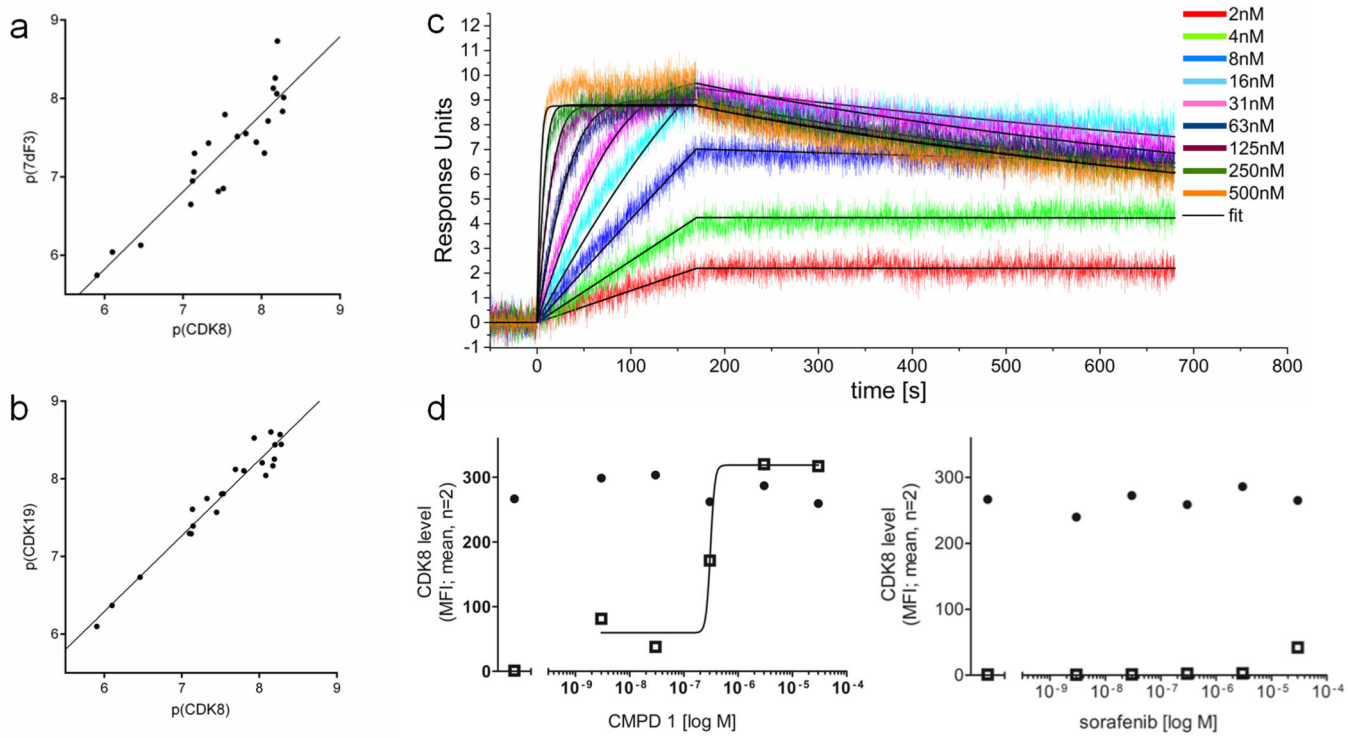

Figure 2. Characterisation of the interaction between CDK8/19 and the 3,4,5-trisubstituted pyridine series

a) CDK8 binding affinity versus 7dF3 cell-based reporter potency for 22 compounds in the 3,4,5-trisubstituted pyridine series (all data shown as pIC_{50}, $R^2 = 0.83$). **b**) CDK8 versus CDK19 binding affinity for 22 compounds in the 3,4,5-trisubstituted pyridine series (all data shown as pIC_{50}, $R^2 = 0.95$). **c)** Direct binding of **1** to CDK8/cyclin C measured by surface plasmon resonance spectroscopy; $K_d = 2$ nM; stoichiometry = 1 : 1; residence time = 11 min. **d**) CETSA analysis confirming target engagement of **1** (left), but absence of sorafenib binding (right), with CDK8 in SW620 cells. Cells were treated with **1** or sorafenib and cell lysates were prepared for analysis after 2 hours treatment. CDK8 levels were determined using a bead-based ELISA: ● non-heated sample; ◘ sample heated at 50°C (n = 2; MFI = Mean Fluorescence Intensity).

Europe PMC Funders Author Manuscripts

Europe PMC Funders Author Manuscripts

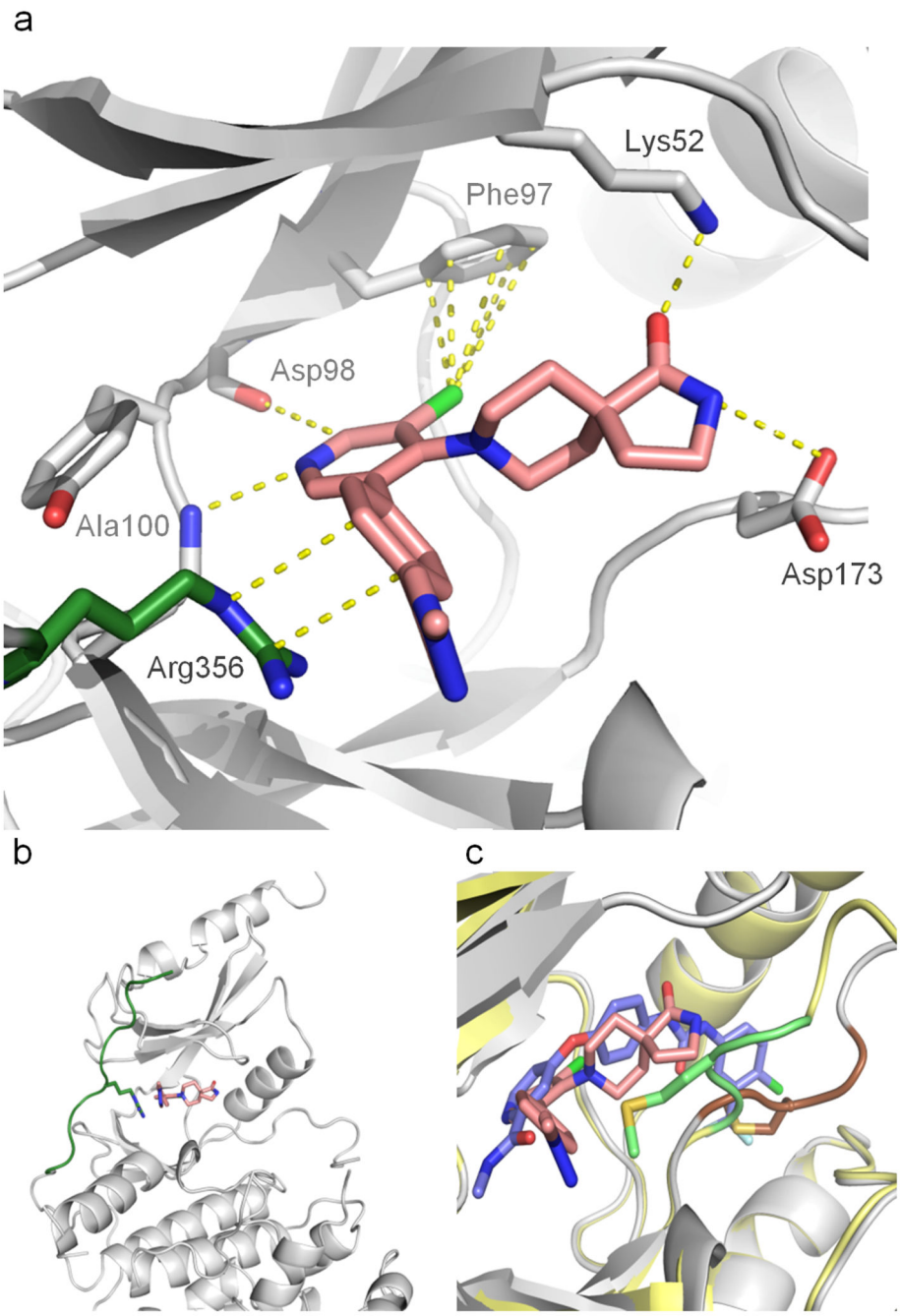

Figure 3. X-ray crystal structural analysis of compound 1 bound to CDK8/cyclin C

a) Protein crystal structure of CDK8/cyclin C bound to **1** (Pdb code: 5BNJ); compound **1** is shown in pink, CDK8 protein in grey with Arg356 highlighted in green; key interactions are depicted by yellow dashed lines and key residues annotated. Residues Lys26, Val27, Gly28, Arg29 and Gly30 have been cropped for clarity. **b**) Protein crystal structure of CDK8/cyclin C bound to **1** showing insertion of C-terminal chain (green) into the hinge region of CDK8. **c**) Protein crystal structure of CDK8 bound to sorafenib (pdb code 3rgf[22]), ligand in purple, protein backbone in light yellow and DMG motif in light green) overlaid with compound **1**

bound to CDK8 (ligand in pink and protein backbone in grey, DMG motif in light brown) showing a DMG-out orientation of the activation loop in the sorafenib-bound structure consistent with a type II binding mode.

Europe PMC Funders Author Manuscripts

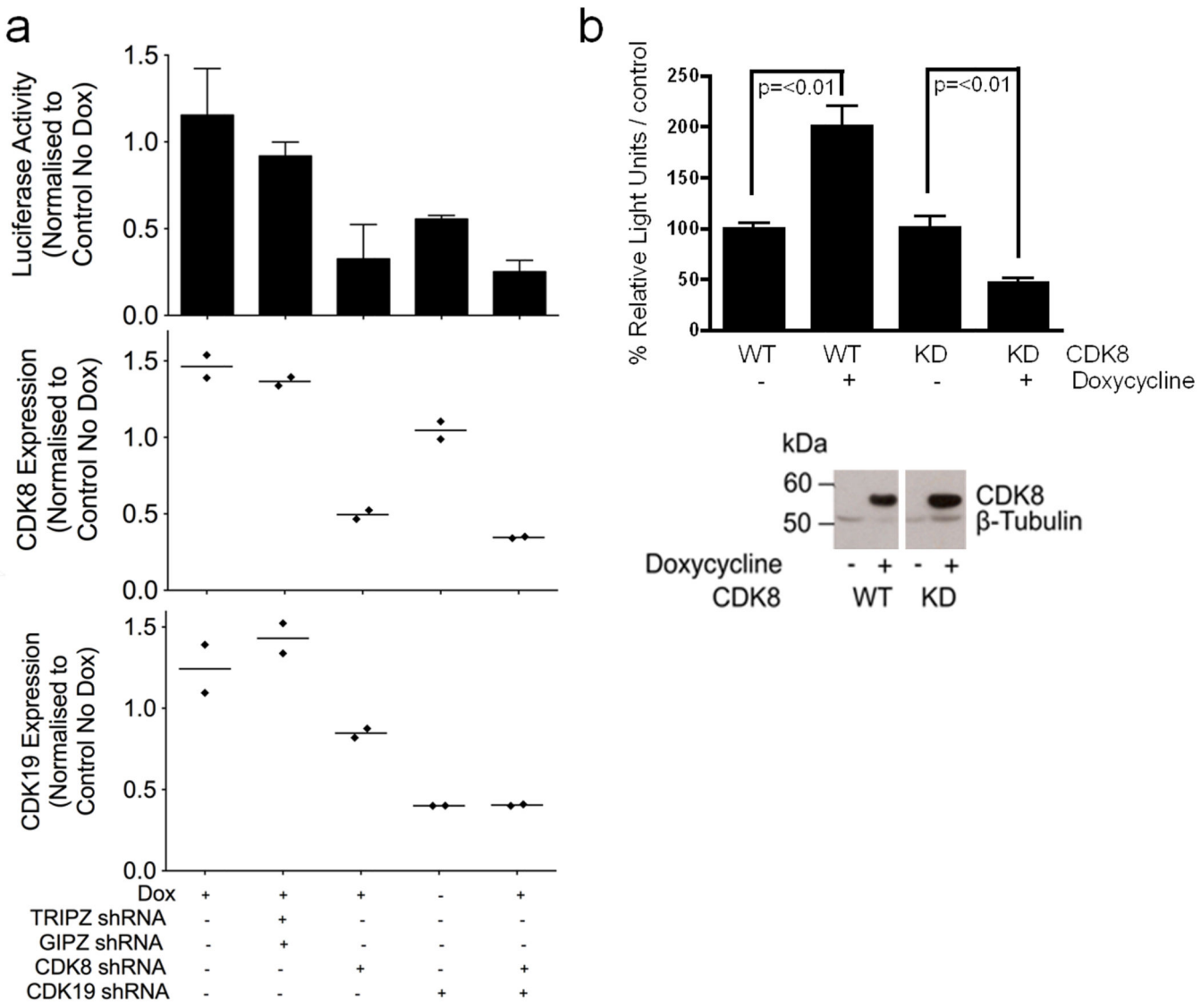

Figure 4. Altered CDK8/19 expression affects WNT-regulated transcription

a) Reduced expression of CDK8, CDK19 or CDK8/19 resulting from shRNA expression inhibits TCF/LEF reporter gene transcription in Colo205 cells (top graph, data represent mean values ± s.e.m, n = 3). Reduced CDK8 and/or CDK19 expression (middle and bottom graph respectively) was confirmed by quantitative RT-PCR. Data is plotted relative to parent cells cultured in the absence of doxycycline (n=2). Cells were treated for 10 days with 5μg/ml doxycycline before reporter or mRNA levels were measured (control dox = parent Colo205 cells, TRIPZ-GIPZ = cells expressing a dox-inducible non-targeting shRNA and also a constitutively expressed non-targeting shRNA, CDK8 = cells expressing a dox-inducible CDK8 shRNA, CDK19 = cells expressing a constitutive CDK19 shRNA and CDK8+CDK19 = cells expressing both a dox-inducible CDK8 shRNA and a constitutive CDK19 shRNA). **b)** Doxycyline-inducible expression of a wild type or a kinase dead CDK8 (D173A) variant (lower immunoblot; Supplementary Fig. 17) induces TCF-dependent reporter transcription in HEK293 cells (upper plot; n=4 ± s.e.m).

Europe PMC Funders Author Manuscripts

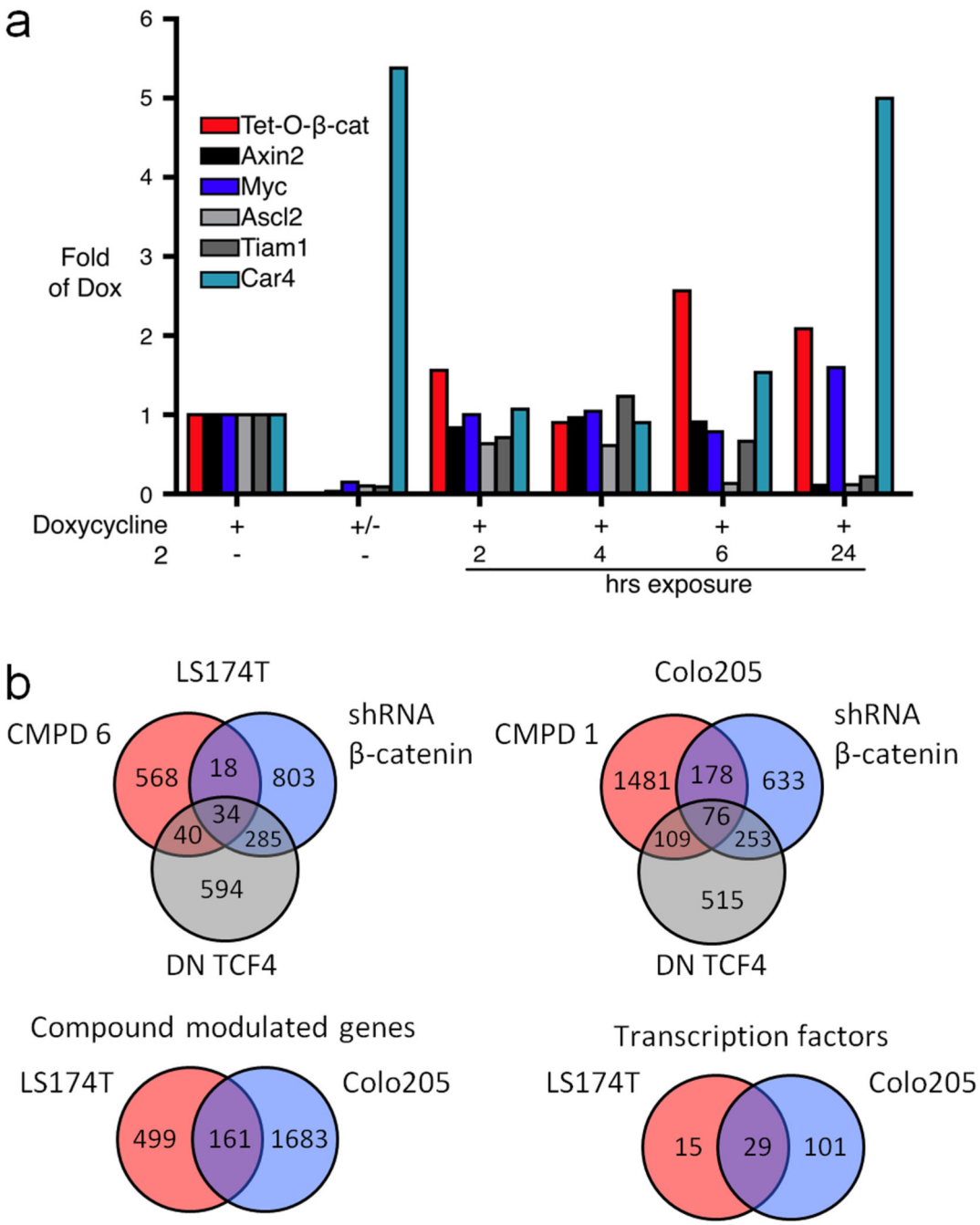

Figure 5. Gene transcript profiling following inhibition of WNT signalling resulting from loss of β-Catenin or following treatment with 3,4,5-trisubstituted pyridines

a) Gene expression in cultured intestinal organoids established from mice expressing a dox-inducible mutant β-catenin (Tet-O-Δ1-89-β-Catenin). Organoids induced with 2mg/ml dox were treated with **2** (2 μM) and transcript levels for WNT target genes (*Myc*, *Ascl2*, *Tiam1* or *Axin2*), the dox-inducible transgene (*Tet-O-β-Catenin*) or the enterocyte differentiation marker *Car4* were then quantified (plot shows a representative experiment; n=1). **b)** Changes in transcript abundance were profiled in LS174T cells in response to a 4 or 24 h treatment

with compound **6** (715nM: IC_{90} for inhibition of the luciferase reporter) and in, Colo205 cells in response to a 2 or 6 h treatment with compound **1** (350 nM). The abundance of 660 and 1844 transcripts were significantly altered in response to treatment of LS174T or Colo205 cells respectively. The upper Venn diagrams show the significant overlap between those transcripts whose expression was altered as a result of compound treatment and those affected by modulation of key WNT regulators, β-catenin or TCF4 (published data[31]; DN TCF4 = dominant negative TCF4). The lower Venn diagrams show the overlap between transcripts modulated as a result of treatment of cells with compounds **1** or **6** (left) and between transcription factors that bind modulated genes in LS174T and Colo205 cells (right).

Europe PMC Funders Author Manuscripts

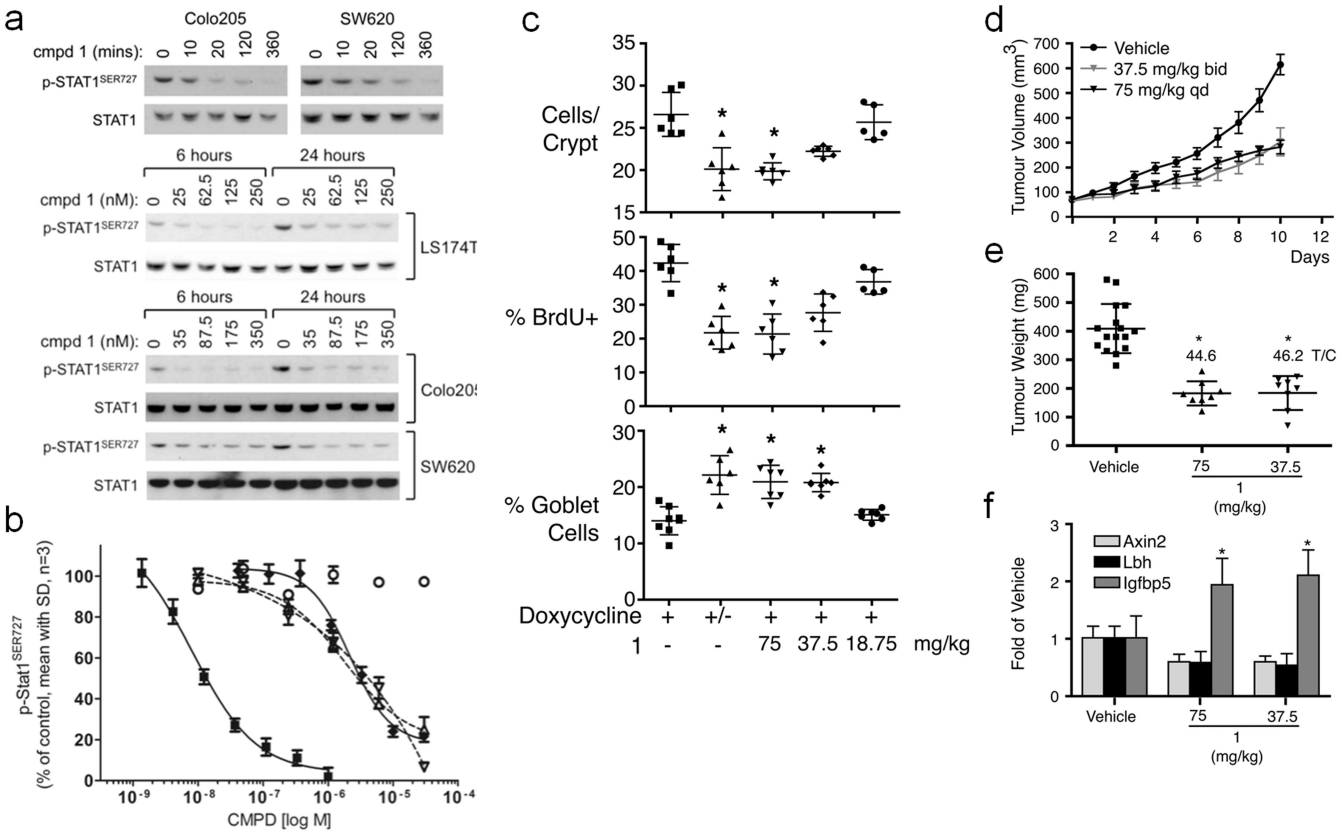

Figure 6. Biomarker modulation and therapeutic effects of compound 1 in human cancer cell lines and *in vivo* animal models

a) Colo205 and SW620 cells were treated for 10-360 min with compound **1** (350 nM: 10x reporter IC_{50}; upper panel). LS174T, Colo205 and SW620 cells were treated for 6 and 24 hours with 1 – 10x their reporter IC_{50} values. Proteins were measured by immunoblotting (Supplementary Fig. 17). **b)** p-STAT1^{SER727} levels were determined following treatment of SW620 cells with **1** (**.** ; IC_{50} = 9nM)**,** sorafenib (○ ; IC_{50} = not determined), ponatinib (Δ ; IC_{50} = 2800nM), linifanib (▿ ; IC_{50} = 1800nM) and less active control **9** (◆ ; IC_{50} = 2200nM, Supplementary Table 9; Mean ± SD; n=3). **c)** Tet-O-β-catenin mice with hyperplastic intestinal epithelium following 6 days dox-treatment were administered with bi-daily **1** for 2 days. Dox-withdrawal was a positive control for loss of WNT signalling. Changes in crypt length, cell proliferation and differentiation (Mean ± SD; n=8) were quantified, * Kruskall-Wallis: P<0.0003; Dunn's post-hoc: P<0.01. **d)** CD1(Nu/Nu) mice bearing MTV-WNT-1 tumours were treated with compound **1** for 10 days and tumour volume estimated from measured dimensions (mean ± SD; n=8; Kruskall-Wallis: P<0.01; Dunn's post-hoc: P<0.05). **e, f)** MTV-WNT-1 tumours were harvested from CD1(Nu/Nu) mice after 10 days treatment and weighed (**e**) or tumour mRNA extracted and the expression of WNT target gene expression or Igfbp5 (involution marker[40]) determined by qRT-PCR (**f**).